Lyotropic and Thermotropic Phase Behavior of Hydrated Monoacylglycerols: Structure Characterization of Monovaccenin†

Hong Qiu and Martin Caffrey*

Department of Chemistry, The Ohio State University, 100 W. 18th Avenue, Columbus, Ohio 43210

Received: December 17, 1997; In Final Form: February 18, 1998

This work is part of a long-term research effort to establish the relationship between lipid molecular structure and lyotropic and thermotropic mesophase propensity by comparing the equilibrium temperature−composition phase diagrams of a homologous series of monoacylglycerols. Here we report the temperature−composition phase diagram of monovaccenin (a C18:1c11 monoacylglycerol) in water, constructed using small-angle X-ray scattering in the temperature range of ca. 0−110 °C and the composition range of ca. 0−60% (w/w) water in the heating direction. The interpreted equilibrium phase diagram is based on several hundred discrete X-ray diffraction measurements in temperature−composition space recorded as a function of temperature in 5 °C increments and of composition in 4% (w/w) water increments on average. The phases identified and characterized structurally in this system include the lamellar crystal phase, the lamellar liquid crystal phase, two inverted cubic phases (Q^{230}, *Ia*3*d*; Q^{224}, *Pn*3*m*), the inverted hexagonal phase, and the fluid isotropic phase. The monovaccenin/water phase diagram is very similar to that of the monoolein (a C18:1c9 monoacylglycerol)/water system. However, there are important differences in transition temperatures and phase boundary positions between the two that we attribute to differences in the effective length and shape of the corresponding amphiphiles. The sensitive response to temperature and lipid identity of the average water channel radius in the fully hydrated, bicontinuous cubic phase makes monoacylglycerol systems important potential candidates for controlled drug release and membrane protein crystallization.

1. Introduction

One of the major objectives in the field of membrane structural biology is to establish the relationship between lipid molecular structure and mesophase (also referred to as liquid crystal) behavior. For purposes of forging such links, we are working with the monoacylglycerols because of their biological and commercial importance, their ready availability, and the rich mesomorphism they exhibit as a function of temperature and hydration. Accordingly, the temperature (*T*)−composition (*C*) phase diagrams for a homologous series of monoacylglycerols are being constructed using X-ray diffraction. The advantage of the diffraction method is that, in addition to mesophase identification, the corresponding phases can be characterized structurally, oftentimes with sub-ångström resolution. Our ultimate goal is to map out the equilibrium *T*−*C* phase diagrams and to compare these and the corresponding mesophase structural features for a series of monoacylglycerols, members of which differ in acyl chain length and double-bond position, to establish the relationship between molecular structure and mesophase behavior. To date, we have reported on three members in the series, monomyristolein (C14:1c9),[1] monopentadecenoin (C15:1c10),[2] and monoolein (C18:1c9)[3] (Figure 1), and work is in progress on monoundecenoin (C11:1ω10), monotridecenoin (C13:1ω12), monopalmitolein (C16:1c9), monoheptadecenoin (C17:1c10), monoeicosenoin (C20:1c11), and monoerucin (C22:1c13).[4]

This paper describes progress made with one member of the series, monovaccenin, which contains a fatty acid, 18 carbon atoms long with a cis double bond at position 11 (C18:1c11) in ester linkage at C1 on the glycerol backbone (Figure 1A.3). It is related to monoolein (C18:1c9, Figure 1A.2), another monoacylglycerol in the series, in that the latter has the cis double bond at C9 while the double bond is at C11 in the former. The phase behavior of the monoolein/water system has been studied extensively (refs 3 and 19 and references therein). On the other hand, no published phase behavior information on the monovaccenin/water system is available. The issue raised in the current study concerns the effect that cis double-bond position has on the thermotropic (temperature-dependent) and lyotropic (in this case, water concentration-dependent) mesomorphism of the monoacylglycerols containing monounsaturated fatty acyl chains, 18 carbon atoms long. The impact of lipid molecular length and shape on phase behavior is discussed.

In this paper, the mesophase behavior and structure characterization of the monovaccenin/water system is reported. The traditional isoplethal (constant composition)-diffraction method was used for this purpose in the 0−110 °C temperature range (in ≤5 °C increments) and in the 0−60% (w/w) water composition range (in increments of ca. 4% (w/w) water). Pure lamellar crystal (L_c) phase, lamellar liquid crystal (L_α) phase, inverted cubic (*Ia*3*d* (Q^{230}), *Pn*3*m* (Q^{224})) phase, inverted hexagonal (H_{II}) phase, and fluid isotropic (FI) phases have been observed as well as two- and three-phase coexistence regions. Our early attempts at constructing the monovaccenin/water phase

† List of abbreviations: α, thermal expansion coefficient; A_0, ratio of the area of the minimal surface in a unit cell to (unit cell volume)$^{2/3}$; β, composition expansion coefficient; χ, Euler−Poincaire characteristic; FI, fluid isotropic phase; Φ_w, volume fraction of water; Φ_l, volume fraction of lipid; η, structure parameter used in determining expansion coefficients; H_{II}, inverted hexagonal phase; IPMS, infinite periodic minimal surface; *l*, lipid length; L_α, lamellar liquid crystal phase; L_c, lamellar crystal phase; r_w, cubic phase water channel radius.

* Corresponding author. Phone: 614-292-8437. Fax: 614-292-1532. E-mail: caffrey@chemistry.ohio-state.edu.

S1089-5647(98)00553-7 CCC: $15.00
Published on Web 05/23/1998

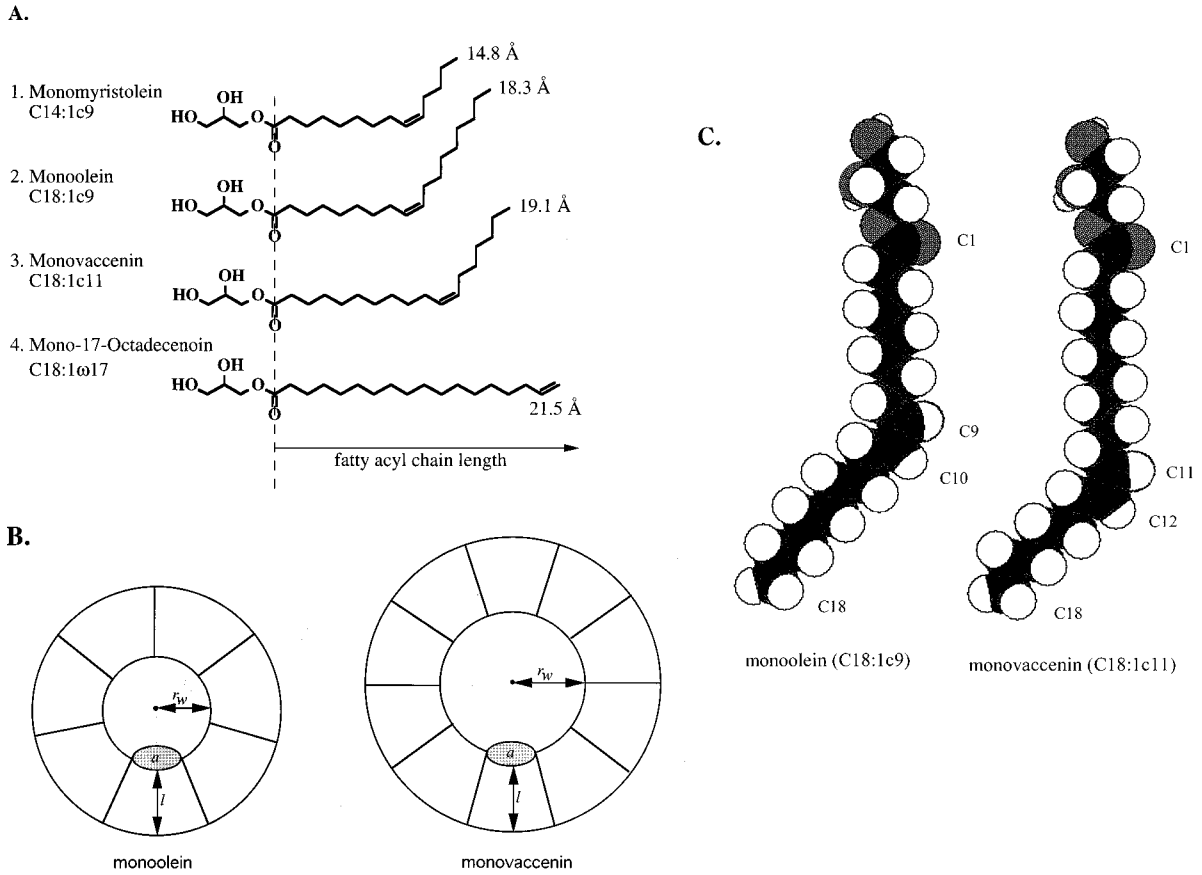

Figure 1. (A) Molecular structure and approximate dimensions of the different monoacylglycerols discussed in the text. A.1, monomyristolein; A.2, monoolein; A.3, monovaccenin; A.4, mono-17-octadecenoin, C18:1ω17. (B) Schematic representation of the water channel and surrounding lipid monolayer in the cubic phase formed by monovaccenin and monoolein where r_w is the water channel radius, a is the molecular headgroup area, l is lipid length, and each wedge-shaped object represents a lipid molecule. For clarity, the water channel and the lipid headgroup are shaded differently. Drawings are purely schematic and are not to scale. (C) Space-filling model of monovaccenin and monoolein. The shading code is as follows: white, hydrogen; gray, oxygen; dark gray, carbon.

diagram lead us to uncover nonequilibrium behavior, especially at temperatures below 25 °C. These observations suggest that the nonequilibrium behavior is shared by other monoacylglycerol/water systems, including the monoolein/water system. This important issue of nonequilibrium and how to avoid it will be discussed. The potential use of cubic phases incorporating the monoacylglycerols in membrane protein crystallization and in controlled release applications will also be addressed in this paper.

2. Materials and Methods

2.1. Materials. Monovaccenin was purchased from Nu Chek Prep Inc. (Elysian, MN). It had a purity of ≥99% as judged by thin-layer chromatography of 1−100 μg monovaccenin run in four solvent systems (petroleum ether/diethyl ether, 94/6 (v/v); petroleum ether/diethyl ether/acetic acid, 75/25/1 (by vol.); chloroform/acetone, 96/4 (v/v); and chloroform/acetone/acetic acid/methanol, 72.5/25/0.5/2 (by vol.) on Adsorbosil Plus 1 plates (Alltech, Deerfield, IL) and was used without further purification. Water was purified by using a Milli-Q Water System (Millipore Corporation, Bedford, MA) consisting of a carbon filter cartridge, two ion exchange filter cartridges, and an organic removal cartridge.

2.2. Sample Preparation. Dry solid monovaccenin (ca. 20 mg) was mechanically mixed with appropriate amounts of water (ca. 1−50 mg) in a syringe-based mixing device as described previously[1,2] to achieve the desired sample composition. Mixing was carried out at room temperature (ca. 25 °C) while preparing the fixed hydration samples ranging from 0 to 60% (w/w) water. The homogeneously mixed samples were then transferred into 1.0 mm diameter quartz capillaries (Charles Supper, Natick, MA), flame-sealed, and glued with 5-min epoxy (Hardman Inc., Belleville, NJ) and were stored prior to data collection at 4 °C for a period ranging from a few days up to 4 weeks. The actual composition of the samples was determined gravimetrically as described[1] with an accuracy of better than 0.1% (w/w) water for low water content samples and 0.5% (w/w) water for high water content samples, using a microbalance (M3P-000V001, Sartorius Corp., Edgewood, NY).

2.3. X-ray Sources. Both synchrotron X-rays (National Synchrotron Light Source (NSLS), Brookhaven National Laboratory) and rotating anode (Rigaku USA Inc., Danvers, MA) copper Kα X-rays were used for diffraction measurements.

The machine energy at NSLS was 2.528 GeV with a typical operating current of ca. 160 mA. Occasionally, 300 mA of current was available. The X-ray beam was focused horizontally at the detector with the second of a double-bounce silicon (111) crystal monochromator and vertically using a nickel-coated aluminum mirror. The X-ray beam energy was 8 keV (1.55 Å) with a flux on the order of 10^{11} photons/s incident on the sample. The beam size at the sample was ca. 6 mm in the horizontal direction and 0.7 mm in the vertical direction. At the detector, which was ca. 300 mm downstream from the sample, the convergent beam measured 0.4 mm in the horizontal and 0.3 mm in the vertical directions.

Copper Kα X-rays (1.54 Å, nickel (0.025 mm-thick) filtered)

were generated using a Rigaku RU-300 rotating anode X-ray generator, operating at 40 kV and 200 mA. A 15 cm long vacuum flight tube fitted with 0.5 mil (0.013 mm)-thick Kapton (Du Pont Electronics, Wilmington, DE) windows was placed between the X-ray shutter and the mirrors. In the line source mode, a 0.5 mm × 10 mm filament was used. The beam was focused vertically by a 6 cm × 2 cm (length × width) nickel-coated glass mirror (Charles Supper, Natick, MA) located ca. 15 cm downstream of the target giving a focal line of 0.3 mm × 20 mm at the detector, which was positioned ca. 40 cm from the mirror. In the point source mode, a 0.5 mm × 10 mm filament was used, and a second mirror was placed downstream of the first mirror to further focus the X-ray beam vertically, giving a focused beam of 2 mm × 0.3 mm at the detector.

2.4. Data Collection. The protocol used to collect data at the synchrotron and on the rotating anode is as follows:

(1) Samples that had been stored at 4 °C were transferred and stored on ice before any measurement was made at the synchrotron. They were subsequently transferred from ice to a beryllium multiple sample holder[1,2] at 0 °C and incubated at each desired temperature in the 0−110 °C range for ca. 30 min (but not less than 20 min). X-ray diffraction patterns were collected at constant temperatures in this range in increments of 5 °C or less in the heating direction on X-ray sensitive film (DEF-5, Kodak, Rochester, NY). The benefit of using synchrotron X-rays to collect data, especially at high temperatures, is that it minimizes exposure and sample incubation times at elevated temperatures where chemical decomposition can be a problem. For this same reason, when incubation temperatures were above 90 °C, the sample incubation time was reduced to 20 min. Typical exposure times were 15 s when the sample-to-film distance was ca. 30 cm.

(2) Copper Kα X-rays in the line and point focus modes were used to collect the diffraction data on samples in the temperature range from 0 to 50 °C in increments of 1−5 °C in the heating direction. The experimental conditions are essentially the same as above except that samples were incubated at −10 °C for 2 h before data collection was started to ensure accessing the L_c phase, and typical incubation times were 4−9 h at the measurement temperature with exposure times of 30 min and 3 h in the line and point focus modes, respectively, and a sample-to-film distance of about 20 cm.

3. Results

3.1. Temperature−Composition Phase Diagram. In this study, great care has been devoted to ensuring that equilibrium phase behavior prevails in the *T*−*C* phase diagram reported for the monovaccenin/water system (Figure 2). The phases identified by X-ray diffraction and their location in temperature−composition space are shown in Figure 2A. Figure 2B shows the phase boundaries and coexistence regions as identified by the diffraction data. For ease of comparison, the latter along with the diffraction data points are presented together in Figure 2C. A schematized view of the diagram is presented in Figure 2D, which serves to identify more clearly the three-phase eutectic and peritectic transitions and the temperatures at which they occur. It was drawn to conform to the experimental data and the Gibbs' phase rule. An expanded view of the data in the 10−30 °C range is shown in Figure 2E.

The pure phases found in this system include the L_c phase, the L_α phase, two inverted bicontinuous cubic phases belonging to space groups *Ia*3*d* and *Pn*3*m*, the H_{II} phase, and the FI phase. The description of the phase diagram that follows is based on the interpreted diagram presented in Figure 2B. Between 0 and 37 °C, the L_c phase exists in a narrow composition range from 0% (w/w) to ca. 1% (w/w) water. Above 37 °C, the dry lipid has fused completely. The melting temperature drops to 30 °C at ca. 4% (w/w) water and rises again with increased hydration reaching a limiting value of ca. 105 °C above 23% (w/w) water. The pure L_α phase region is roughly triangular in shape with 5% (w/w) water at ca. 30 °C, 27% (w/w) water at 20.5 °C, and the upper apex at 10% (w/w) water and 60 °C. The pure *Ia*3*d* phase is found in samples ranging from ca. 48% (w/w) water at 19.5 °C, ca. 23% (w/w) to 38% (w/w) water at 40 °C, and between 10% (w/w) and 28% (w/w) water at 60 °C. It has an upper temperature limit of ca. 85 °C at ca. 24% (w/w) water. Moving to higher hydration levels, between 34% (w/w) and 39% (w/w) water, the pure *Pn*3*m* phase is identified at 50 °C, which is in the middle of a long narrow stretch of pure *Pn*3*m* phase that extends from 15.5 °C to ca. 87 °C. At 80 °C, this pure cubic phase region is located between 25% (w/w) and 29% (w/w) water. At higher temperatures, the cubic phases give way to the H_{II} phase, identified in samples containing greater than ca. 20% (w/w) water between ca. 83 and 105 °C. The hydration boundaries of the FI and H_{II} phases both exist in the 21% (w/w) to 26% (w/w) water region, as defined by the composition dependence of the corresponding structure parameter (Figure 3B).

Extensive phase coexistence is a prominent feature of the *T*−*C* phase diagram for the monovaccenin/water system. Coexistence of the L_c and FI phases is observed in a triangular shaped region with a low-temperature limit of ca. 30 °C from 1% (w/w) to 4% (w/w) water and an apex at ca. 37 °C for the dry lipid. The L_α and *Ia*3*d* phases coexist between 27% (w/w) and 46% (w/w) water at 20.5 °C. This coexistence region has an upper temperature limit of 60 °C at 10% (w/w) water. *Ia*3*d* and FI phases are found coexisting from 60 °C up to 83 °C at 10% (w/w) and 20% (w/w) water, respectively. A long and narrow s-shaped region of *Ia*3*d* and *Pn*3*m* phase coexistence was identified between the two pure phases that extends from 19.5 to 85 °C. In the excess water region, the *Pn*3*m* phase coexists with bulk water between ca. 15 °C and ca. 87 °C at hydration values above 52% (w/w) and 29% (w/w) water, respectively. The H_{II} phase coexists with water between 87 and 105 °C above ca. 25% (w/w) water, and the FI phase coexists with excess water above 105 °C and ca. 23% (w/w) water. Because of difficulties in defining precisely the compositional width of the pure L_c phase, the L_c-excess water coexistence region is assumed to extend from ca. 1% (w/w) water in the 0−15.5 °C range. At least two polymorphs have been observed in the L_c region that are recognizable by their distinct wide-angle diffraction patterns. This aspect of monovaccenin phase behavior was not examined carefully and will not be discussed further in this report. Coexistence of H_{II} and *Ia*3*d*, H_{II} and *Pn*3*m*, and L_α and FI phases was also found along the respective shared phase boundaries. While coexistence of the H_{II} and FI phases was not detected experimentally, it must exist and is so indicated in Figure 2 to be consistent with the Gibbs phase rule.

Early measurements performed in this study using temperature increments of 5 °C showed that phase behavior in the region between 10 and 25 °C over the entire composition range studied is complicated. To define more precisely the phase diagram in this region, additional measurements were made in increments of 1 °C between 15 and 23 °C (see Figure 2E). Two types of phase coexistence have been identified here. Specifically, the L_c and *Pn*3*m* phases coexist beginning at 15.5 °C. As temperature rises to ca. 19.5 °C, the coexisting phases are of

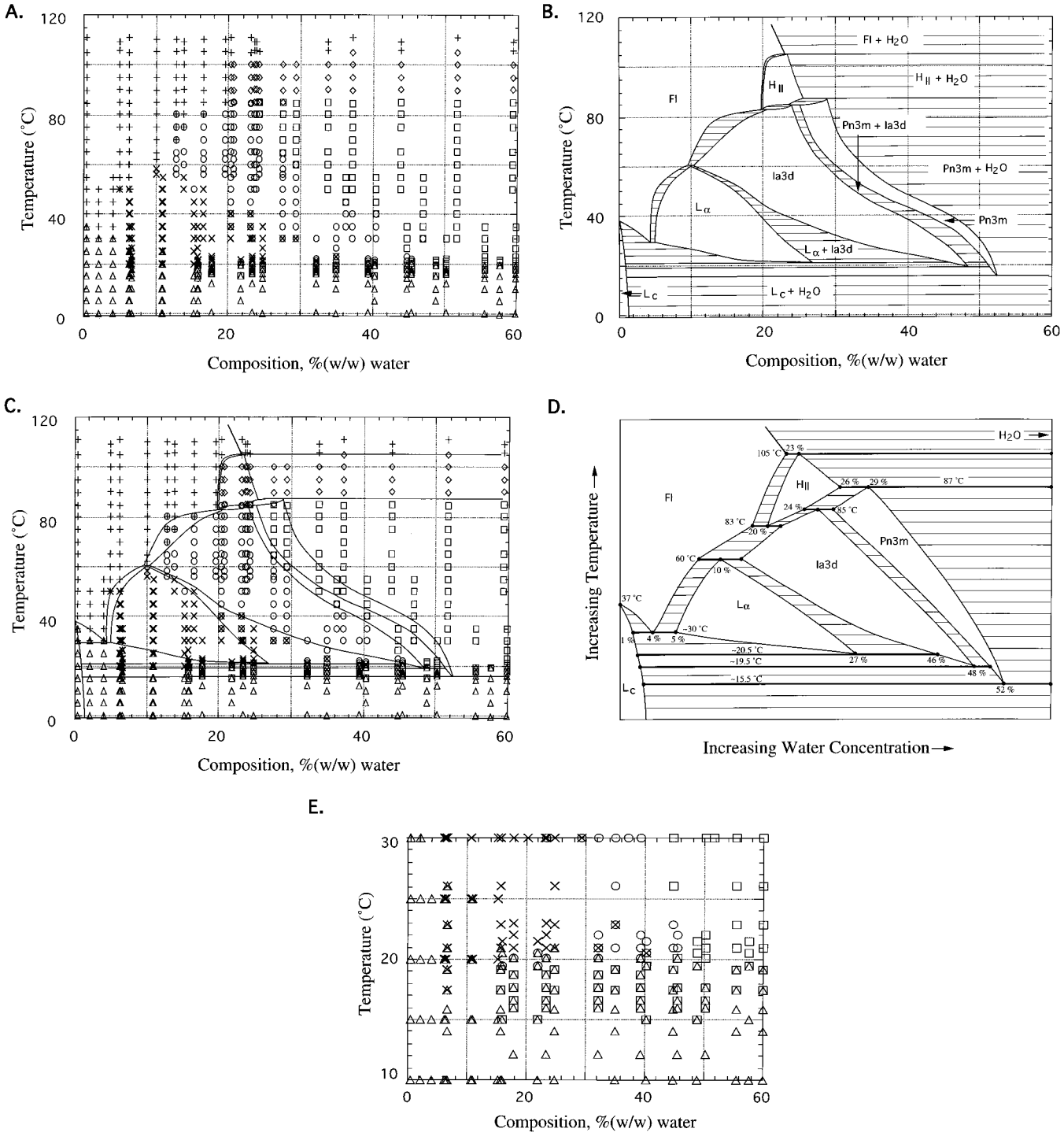

Figure 2. (A) Identity and location in temperature−composition space of each phase and coexisting phases in the monovaccenin/water system as determined by X-ray diffraction in the heating direction. The identity of the phases is as follows: (+) Fl, (△) L_c, (◇) H_{II}, (○) cubic-*Ia3d*, (□) cubic-*Pn3m* and (×) L_α. (B) Temperature−composition phase diagram of the monovaccenin/water system based on an interpretation of the data in Figure 2A and the hydration data in Figure 3B. (C) Superposition of the diffraction data in Figure 2A and the interpreted phase diagram in Figure 2B. The narrow (Fl + H_{II}) phase coexistence region in Figure 2B has not been verified experimentally but is so positioned to follow the Gibbs phase rule. The location (composition) of the cubic phase hydration boundary was estimated and verified as described.[3] In the dry state, the L_c phase of monovaccenin exists in several polymorphic forms as evidenced by differences in chain-packing characteristics (wide-angle region of the diffraction pattern). The same holds in the presence of added water, and thus, the L_c phase, as identified in this region of the diagram, corresponds to a number of different polymorphs. (D) Schematized view of the diagram in Figure 2C to reveal the nature of the assorted eutectic (at ca. 15.5, 19.5, 20.5, 30, and 83 °C) and peritectic (at 60, 85, 87, and 105 °C) transitions and the temperatures and compositions at which they occur. The temperature and composition values included in this figure identify important transitions and phase coexistence regions reported in Figure 2B. The lines connecting these temperature−composition coordinates are drawn schematically. (E) Expanded view of the 10−30 °C data in Figure 2A.

the L_c and *Ia3d* type. These data suggest that the system behaves as indicated in Figures 2 and 5A.

3.2. Mesophase Expansion Coefficients. The temperature and composition dependence of the unit cell dimension of the different mesophases found in the phase diagram of the monovaccenin/water system presented above are shown in Figure 3. The lattice parameter of all liquid crystalline phases examined decreases with increasing temperature (Figure 3A),

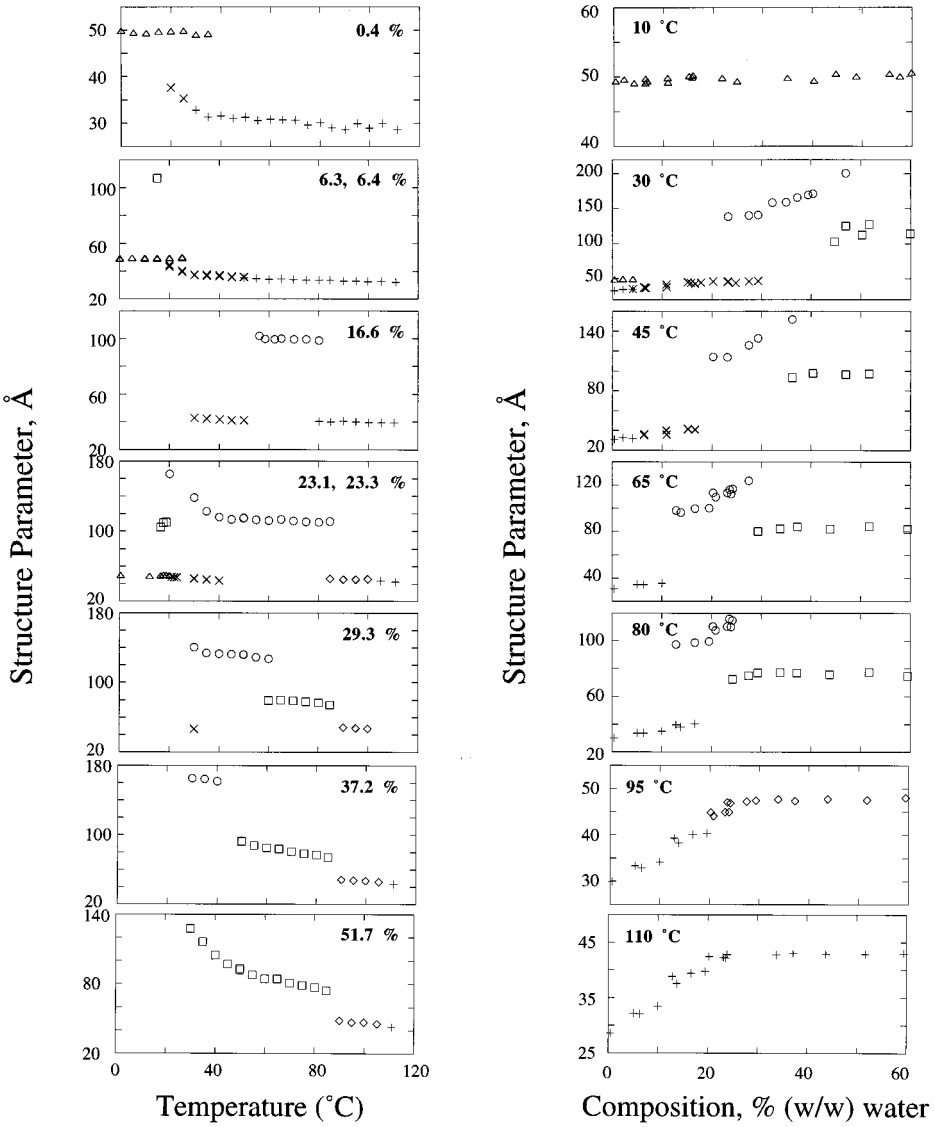

Figure 3. Temperature (A, left) and composition (B, right) dependence of the structure parameters of the phases found in the monovaccenin/water system at the indicated overall sample compositions in units of % (w/w) water and at selected temperatures. The structure parameter values reported are accurate to ±0.3 Å for all of the phases. The identity of the phases is as follows: (△) L_c, (×) L_α, (○) cubic-*Ia*3*d*, (□) cubic-*Pn*3*m*, (◇) H_{II}, and (+) FI. Because of the very small difference in composition, we have taken the liberty of including the structure parameter temperature-dependence data recorded at 6.3 and 6.4% (w/w) water in the same plot. The same holds for the 23.1 and 23.3% (w/w) water data.

while that of all pure mesophases increases with increasing sample hydration (Figure 3B). This behavior is expected and typical for the liquid crystalline phases of lipid/water systems and can be quantified as the thermal and composition expansion coefficients, α and β, respectively, defined as follows

$$\alpha = \frac{1}{\eta}\frac{\Delta\eta}{\Delta T} \quad (1)$$

and

$$\beta = \frac{1}{\eta}\frac{\Delta\eta}{\Delta W} \quad (2)$$

where $\Delta\eta/\Delta T$ and $\Delta\eta/\Delta W$ represent the slope of a straight line fit to the temperature and composition dependence of the lattice parameters of the different phases over a limited temperature and composition range, respectively. η is the lattice parameter of the phase calculated from the equation of the aforementioned fitted line at a specified temperature or composition. α- and β-values for the monovaccenin phases range from ca. -1 to -6 kK^{-1} and from ca. 100 to 250 ppm^{-1}, respectively (Table 1). Because the *pure Pn*3*m* phase exists only over a very narrow composition range at any fixed temperature (Figure 2), there were insufficient data upon which to base a reliable determination of the composition expansion coefficients for this phase. The reported thermal and composition expansion coefficients are typical of what has been measured for the mesophases identified in related hydrated monoacylglycerols.[1−3]

4. Discussion

4.1. Equilibrium Verification. Considerable effort has gone into verifying that the behavior presented in the phase diagram shown in Figure 2 represents equilibrium. We have used adherence to the phase rule and the lever rule as criteria for equilibrium.

For a two-component system, as represented by monovaccenin in water, the phase rule takes the form $3 - P = F$, where P is the number of phases that can coexist at equilibrium and F is the number of variables. In this case, pressure is considered to be a constant at 1 atm. Thus, a maximum of three phases ($P = 3$, $F = 0$) can coexist simultaneously at equilibrium. Such

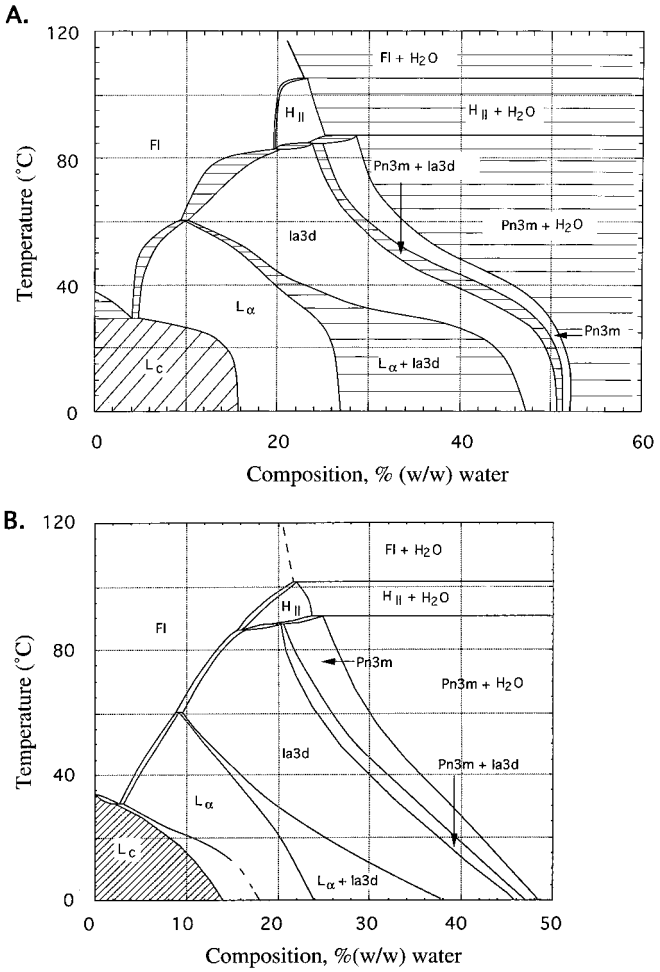

Figure 4. (A) Temperature−composition diagram of the monovaccenin/water system as determined by X-ray diffraction in the heating direction, based on diffraction data obtained from synchrotron measurements. The lower right-hand corner of the diagram (extending from 10% to 60% (w/w) water and from 0 °C to 30 °C) shows undercooling of the L_α, *Ia*3*d*, and *Pn*3*m* phases when compared with the equilibrium phase diagram shown in Figure 2. (B) Temperature−composition diagram of the monoolein/water system in the composition range from 0% to 48% (w/w) water, and in the temperature range from 0 to 102 °C in the heating direction, as obtained by X-ray diffraction.[3]

a three-phase region in the phase diagram must exist either as a point or as a horizontal line and be temperature invariant. For example, in Figure 2B, a horizontal line separates the (*Pn*3*m* + H_2O) and (H_{II} + H_2O) coexistence regions at 87 °C, where the *Pn*3*m*, H_{II}, and excess water phases coexist. Similarly, horizontal lines are included in Figure 2 that represent (H_{II} + FI + H_2O) coexistence at 105 °C, (H_{II} + *Ia*3*d* + *Pn*3*m*) coexistence at 85 °C, (FI + H_{II} + *Ia*3*d*) coexistence at 83 °C, (FI + L_α + *Ia*3*d*) coexistence at 60 °C, (L_c + FI + L_α) coexistence at 30 °C, (L_c + L_α + *Ia*3*d*) coexistence at 20.5 °C, (L_c + *Ia*3*d* + *Pn*3*m*) coexistence at 19.5 °C, and (L_c + *Pn*3*m* + H_2O) coexistence at 15.5 °C. In the two-phase coexistence regions (where $P = 2$, $F = 1$), such as that represented by the (L_α + *Ia*3*d*) coexistence region in Figure 2, specifying temperature is sufficient to fully define the phase. In the pure or single-phase regions (where $P = 1$, $F = 2$), both temperature and composition are variables, and both must be specified to define phase behavior. Consistent with this requirement is the observation that the dimension of a given single phase increases isothermally with sample hydration (Figure 3B).

The lever rule requires that the composition of two coexisting phases remains constant while the relative amounts of the two

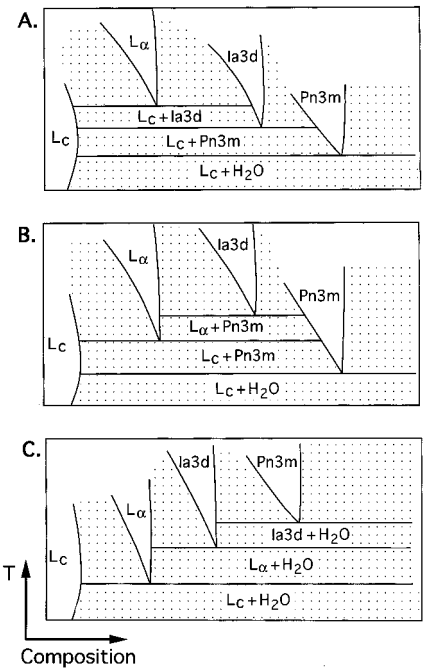

Figure 5. Schematized view of the monovaccenin/water phase diagram in the 0 to 25 °C range. The three transitions shown take place over a relatively narrow temperature range of 5 °C (see Figure 2D). Three sequences in which the transitions can occur with increasing temperature are illustrated. That shown in (A) is consistent with the experimental data (Figure 2E). Shaded regions indicate phase coexistence.

phases change as the overall composition of the sample is varied at any fixed temperature. Such behavior is reflected in the monovaccenin/water system as a constant lattice parameter corresponding to a phase of fixed composition for each of two coexisting phases while overall sample hydration is changed isothermally (Figure 3B). Thus, for example, along the 30 °C isotherm, the L_c and FI lattice parameters remain essentially constant at 49 and 35 Å, respectively, throughout the two-phase coexistence region in the range from 0.4% (w/w) to 4% (w/w) water. The same is true for (L_α + *Ia*3*d*) phase coexistence in the 23% (w/w) to 29% (w/w) water region, where the L_α and *Ia*3*d* phases have constant lattice parameters of 46 and 140 Å, respectively. At higher temperatures, the limited overall composition range in which coexistence prevails makes it difficult to evaluate this aspect of the lever rule. The rule is very obviously obeyed where the L_c, *Pn*3*m*, H_{II}, and FI phases, respectively, coexist with excess water, as evidenced by the constant lattice parameter at high hydration levels (Figure 3B).

The observation that the data in Figure 2 are in agreement with the phase rule and the lever rule corroborates the general view that equilibrium behavior prevails throughout most of the monovaccenin/water $T-C$ phase diagram shown in Figure 2. Differential scanning calorimetry (DSC) data collected on this system (to be reported on separately) support this conclusion.

4.2. Nonequilibrium Phase Behavior. Early attempts at constructing the $T-C$ phase diagram for the monovaccenin/water system were based on protocols developed with monoolein.[3] Here, samples were preincubated at 0 °C prior to data collection (see Data Collection). Following this procedure, the monovaccenin/water $T-C$ diagram shown in Figure 4A was obtained. Comparison of Figure 4A and Figure 2B shows that the two diagrams differ dramatically below 30 °C. We have since determined that the behavior represented in Figure 4A in the low-temperature region arises owing to an undercooling of the three liquid crystal phases. To reset the system into the

TABLE 1: Values of and Parameters Used in Determining the Thermal (α) and Compositional (*β*) Expansion Coefficients of the Different Phases in the Monovaccenin/Water System

phase	temp (°C)[a]	composition, % (w/w) water[b]	equation of best fit[c]	η (Å)[d]	α (kK^{-1})[e]	β (ppm^{-1})[f]
L_α	35 (20−50)	15.2	$d = 52.1 - 0.2467T$ (0.987)	43.5	−5.67	
*Ia*3*d*	45 (35−50)	29.3	$d = 138.5 - 0.1286T$ (0.991)	132.7	−0.97	
*Pn*3*m*	75 (65−80)	29.3	$d = 94.1 - 0.21493T$ (0.997)	77.9	−2.76	
H_{II}	95 (90−100)	23.6	$d = 56.6 - 0.0973T$ (0.9999)	47.4	−2.05	
FI	95 (55−110)	6.3	$d = 37.2 - 0.0452T$ (0.973)	32.9	−1.38	
L_α	30	17 (6−20)	$d = 33.1 + 0.6470W$ (0.942)	44.1		147
*Ia*3*d*	56	21 (20−28)	$d = 53.4 + 2.6134W$ (0.986)	108		242
H_{II}	90	23 (20−24)	$d = 31.9 + 0.6260W$ (0.705)	46.3		135
FI	90	10 (0−17)	$d = 28.7 + 0.7279W$ (0.977)	35.9		202

[a] Temperature at which the thermal expansion coefficient was evaluated. The temperature range (T_1-T_2) over which the temperature dependence of the lattice parameter was fit is indicated in parentheses. [b] Sample composition at which the compositional expansion coefficient was evaluated. The composition range (C_1-C_2) over which the composition dependence of the lattice parameter was fit is indicated in parentheses. [c] Equation of the straight line best describing the temperature or composition dependence of the lattice parameter in the range indicated. The units of *d*, *T*, and *W* are Å, °C and % (w/w) water, respectively. The correlation coefficient, *R*, of the fitted line is shown in parentheses. [d] η is the lattice parameter calculated at the temperature or composition indicated and used in determining the thermal or compositional expansion coefficient. [e] The thermal expansion coefficient α is defined as $(1/\eta)(\Delta\eta/\Delta T)$, where $\Delta T = T_2 - T_1$ and kK^{-1} = [kilokelvin]$^{-1}$. [f] The compositional expansion coefficient β is defined as $(1/\eta)(\Delta\eta/\Delta W)$, where $\Delta W = C_2 - C_1$ and ppm^{-1} is [parts per million (w/w) water]$^{-1}$.

equilibrium L_c phase at low temperatures, we preincubate the sample at −10 °C for at least 2 h. Regardless of hydration, this protocol consistently returns the sample to the L_c phase. Accordingly, this "subzero" (degree Celsius) preincubation protocol was implemented in constructing the diagram shown in Figure 2 as described under Materials and Methods.

Separate calorimetry measurements on the monovaccenin/water system support the claim that the diagram in Figure 2 represents equilibrium behavior (unpublished data). Additional measurements on the monoolein/water system suggest that its phase behavior at low temperature is similar to that of monovaccenin as shown in Figure 2. Thus, this region of the monoolein/water phase diagram (Figure 1 in ref 3) represents nonequilibrium behavior. Work on establishing the equilibrium phase behavior for the latter system is in progress.

4.3. Water Channel Radius and Lipid Length in Cubic Phases. The bicontinuous nature of lipidic cubic phases[5] has attracted considerable attention in the areas of controlled release,[6] crystallization,[7−10] and biosensor design.[11] Applicability is purported to depend on the water channel and lipid bilayer dimensions of these inverted cubic phases. Accordingly, we have set about calculating the pore size (diameter) of the water channels that permeate the cubic mesophase, using two methods. The first invokes the infinite periodic minimal surface (IPMS) model. In this model, the surface where the terminal methyl groups of acyl chains from adjacent lipid monolayers meet defines the IPMS. Since we are dealing with inverted mesophases, the cross-sectional area per lipid molecule is a maximum at the minimal surface and decreases progressively along the length of the hydrocarbon chain to reach a minimum value at the glycerol headgroup. The projected cross-sectional area reduces to zero at the center of the water channel.

For a cubic phase of the type under discussion, Anderson[12] has shown that the molecular cross-sectional area evaluated on a surface parallel to and at a distance, ξ, from the minimal surface and integrated over one of the two monolayers within the unit cell, $A(\xi)$, is related to the experimentally measurable lattice parameter, *a*, as follows

$$A(\xi) = A_0 a^2 + 2\pi\chi\xi^2 \qquad (3)$$

where A_0 and χ are the ratio of the minimal surface in a unit cell to the quantity (unit cell volume)$^{2/3}$ and the Euler−Poincare characteristic, respectively, and have values specific to the different cubic phases (*Ia*3*d*: $A_0 = 3.091$, $\chi = -8$; *Pn*3*m*: $A_0 = 1.919$, $\chi = -2$).[12] Equation 3 can be used to estimate the water channel radius as follows. As noted, at the center of the water channel, where ξ is the sum of water channel radius, r_w, and lipid length, *l*, $A(\xi)$ reduces to zero at the center of the water channel. By making the appropriate substitutions relevant to the *Pn*3*m* phase, eq 3 reduces to

$$r_w = 0.391a - l \qquad (4)$$

Thus, r_w can be determined by measuring *a* and by calculating the corresponding value of *l* using eq 5 (below). We note that the r_w values obtained by using eq 4 are estimates. Owing to the assumption that the center of the water channel runs parallel to the minimal surface, there are systematic errors in the calculations of r_w.

In the IPMS model, *l* can be calculated for the pure cubic phases using the lattice parameter, *a*, determined by X-ray diffraction, the known sample composition, Φ_l, (% (w/w) lipid), and by using the following relation[13]

$$\Phi_l = 2A_0\left(\frac{l}{a}\right) + \frac{4\pi\chi}{3}\left(\frac{l}{a}\right)^3 \qquad (5)$$

It is assumed that the partial specific volume of the lipid and water components of the system are equal and independent of temperature and composition in the range studied and that *l* is temperature-dependent but independent of composition and cubic phase type for a given lipid system.[2,3] The values of *l*, calculated for the pure cubic phases over a range of compositions, have been plotted against temperature (Figure 6), and the corresponding data were fitted with the following exponential (correlation coefficient = 0.82)

$$l = 18.7e^{(-0.0026T)} \qquad (6)$$

where *T* and *l* have units of °C and Å, respectively.

As an alternative to the preceding IPMS analysis, r_w was also calculated using a geometric approach.[14] In this analysis, the inverse bicontinuous cubic phases are described as forming two mutually interwoven and unconnected networks of water-filled rods of finite length. Individual rods are joined tetrahedrally in the case of the *Pn*3*m* phase. If the lattice parameter of the cubic unit cell, *a*, and the volume fraction of water, Φ_w, (assuming $\rho_l = \rho_w$) are known, the water channel radius of the *Pn*3*m* phase, r_w, can be determined by solving the following relationship for r_w

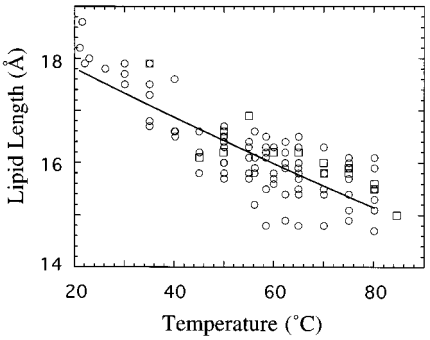

Figure 6. Temperature-dependence of the lipid length calculated for the pure cubic phases found in the monovaccenin/water system. The data were fitted with the following exponential: $l = 18.7e^{(-0.0026T)}$ where T is temperature in °C and l is lipid length in Å. The correlation coefficient is 0.82. Circles and squares correspond to the *Ia*3*d* and *Pn*3*m* phases, respectively.

$$\Phi_w a^3 = 4\pi r_w^2 l_r (1 - 0.78 r_w/l_r) \quad (7)$$

where l_r is the length of each rod, and $l_r = \lambda = a\sqrt{3}/2$ for the *Pn*3*m* phase.[14]

The water channel radius of the *Pn*3*m* phase in fully hydrated (up to 60% (w/w) water) monovaccenin in the temperature range of 40−85 °C has been calculated using both IPMS and geometric approaches. The results are shown in Figure 7 along with the corresponding r_w values for the fully hydrated *Pn*3*m* phase in the monomyristolein (C14:1c9) and monoolein (C18:1c9) systems. In all cases, the geometric method yields r_w values consistently lower by 1−2 Å than the IPMS method as noted previously.[3] For monovaccenin, the water channel radius dimension is bracketed by that of the monomyristolein and monoolein systems and ranges from ca. 24 Å at 40 °C to 14 Å at 80 °C (Figure 7).

Before beginning the phase behavior study of monovaccenin, we expected this lipid to have a longer effective chain length, and thus, a smaller water channel in the fully hydrated *Pn*3*m* phase, than monoolein, on the basis of the following rationale. Monovaccenin has an 18-carbon fatty acyl chain with a cis double bond at carbon number 11, while monoolein, with the same number of carbon atoms, has the cis double bond at the C9 position. If the molecular structure of these lipids, as drawn in Figure 1A, reflects in any way the conformation of the respective molecules in the different phases, then shifting the double bond toward the methyl end of the chain and away from the polar headgroup should increase what we refer to as the effective length of the molecule, l (Figure 1B). The latter effect is seen fully developed in the case of the homologue shown in Figure 1A.4 where the double bond is at the ω-terminus of the acyl chain. As noted earlier,[3] shortening the acyl chain provides for a larger hydrophilic or aqueous channel in the fully hydrated inverted bicontinuous mesophase (compare data in Figure 7 for C14:1c9 and C18:1c9). This simple logic leads to the conclusion that monovaccenin, with its longer effective chain length, is expected to have a *smaller* water channel than monoolein.

The X-ray diffraction data on the monovaccenin/water system is not consistent with this reasoning (Figure 7). Rather, it shows that monovaccenin in the fully hydrated *Pn*3*m* phase has a slightly bigger water channel than monoolein at all temperatures. At 50 °C, the water channel radius of monovaccenin is ca. 3 Å larger than that of monoolein. The difference between them lessens as temperature increases, reaching a value of ca. 1 Å at 80 °C. Even though the IPMS and geometric approaches used to calculate water channel radius do not give exactly the same

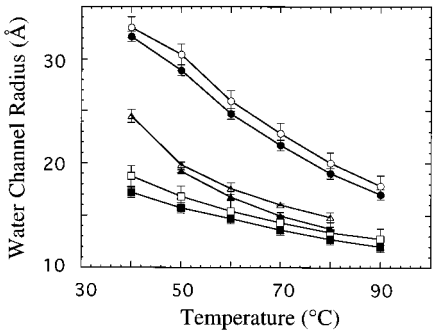

Figure 7. Temperature dependence of the water channel radius of fully hydrated monovaccenin (C18:1c11, triangles), monoolein (C18:1c9, squares),[3] and monomyristolein (C14:1c9, circles)[1] in the *Pn*3*m* cubic phase. The open symbols represent the water channel radius calculated using the IPMS approach according to eq 4. The closed symbols show the water channel radius calculated using the geometric approach according to eq 7. Lines are drawn to guide the eye.

results, both indicate that monovaccenin has a slightly bigger water channel than monoolein. Following the lipid length−water channel relationship developed previously[3] and presented above, the effective lipid length of monovaccenin should be *shorter, not longer*, than that of monoolein.

We must now reconcile the disparity between the prediction and the result. Let us begin by considering lipid length. The molecular structures in Figure 1A reflect more the state of the rigid lipid chains in the solid L_c phase in contrast to the disordered chain arrangement of the liquid crystalline cubic phase. Thus, the lipid length difference caused by shifting the double-bond position by two methylene groups toward the methyl end of the acyl chain might not be seen in the cubic phases, where the effect is likely to be "washed out" by chain disorder. Indeed, this is the case. The calculated lipid length in the cubic phases of these two lipids is not significantly different. The lipid length temperature dependence of monoolein is described by the relationship $l = 18e^{(-0.0019T)}$ (correlation coefficient, 0.93),[3] while that for monovaccenin is $l = 18.7e^{(-0.0026T)}$ (correlation coefficient, 0.82, Figure 6). The corresponding l values differ by less than 0.3 Å for the two lipids in the 50−80 °C range. Given that the error associated with l is in the range of 1 Å, a difference of 0.3 Å is not significant. Thus, to within the sensitivity of the current methods, we conclude that monovaccenin and monoolein have about the same lipid length in the relevant temperature range. If so, we must now explain the observed difference in water channel radius between the two systems (Figure 7).

The original prediction of Briggs et al. (1996) was based on a comparison of two lipids, monoolein (C18:1c9) and monomyristolein (C14:1c9). Both lipids have the cis double bond at the C9 position. This prediction however, does not consider the overall shape of the lipid, which can be described qualitatively by the shape factor, γ ($=v/a(l)l$,[15] where $a(l)$ is the molecular headgroup area and v is the molecular volume). In the inverted cubic phase, γ is >1. In an unsaturated monoacylglycerol, the presence of a cis double bond in the acyl chain creates a kink or bend in the molecule, the magnitude of which depends on the location of the double bond, as illustrated in Figure 1A. Accordingly, the dynamically averaged length of the molecule will change depending on the position of the double bond. Thus, moving it from C9 to C11, in going from monoolein to monovaccenin, has the effect of generating a "slimmer" molecule with a correspondingly smaller γ. A smaller γ, which is still greater than unity in this case, is consistent with a less highly curved polar/apolar interface that

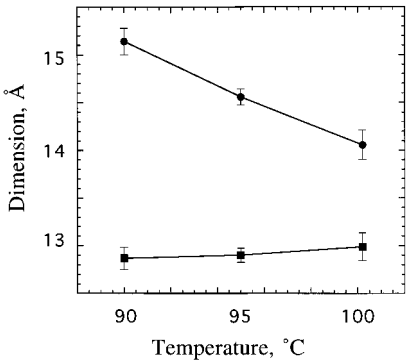

Figure 8. Temperature dependence of the water channel radius and lipid length of fully hydrated monovaccenin in the H_{II} phase. The circles and squares represent, respectively, the water channel radius calculated according to eq 8 and the lipid length calculated according to eq 9. Lines are drawn to guide the eye. Radius and length values were calculated as the average (±standard deviation) for seven samples in the excess water region at the indicated temperatures.

envelopes a larger sized water channel as shown in Figure 1B. This altered shape would account for the observed increase in r_w for monovaccenin compared to monoolein (Figure 7). We must conclude therefore that while relocating the cis double bond two methylene units closer to the methyl terminus of the chain has a negligible effect on lipid length in the cubic phase, it does impact on the dynamically averaged shape of the lipid molecule. The net effect is to create a molecular shape that is less exaggerated in splay along its length and that, upon packing in the inverted cubic phase geometry, has a less curved polar/apolar interface and a larger aqueous channel size. Thus, we see the need to consider *both lipid length and lipid shape* when evaluating how molecular structure impacts on mesophase geometry.

4.4. Water Carrying Capacity. As temperature increases, monovaccenin eventually enters the H_{II} phase from the *Pn*3*m* phase, as was observed with hydrated monoolein. To compare the dimensions of the polar and apolar compartments within the *Pn*3*m* and H_{II} phases quantitatively, the water channel radius and lipid length of the inverted hexagonal phase under conditions of full hydration were calculated using the geometric approach[16]

$$R_w^2 = \frac{2d_{hex}^2\Phi_w}{\sqrt{3}\pi} \tag{8}$$

and

$$l = \frac{d_{hex}}{\sqrt{3}} - R_w \tag{9}$$

where d_{hex} is the lattice parameter of the H_{II} phase (interplane distance) and Φ_w represents sample water content at the hydration boundary (expressed as a fractional volume, assuming $\rho_l = \rho_w$). The latter is obtained from the data presented in Figure 3B (see plot at 95 °C, where the structure parameter of the H_{II} phase becomes independent of hydration). The corresponding data (not shown) at 90 and 100 °C show that the hydration boundary of the H_{II} phase is relatively insensitive to temperature. Φ_w values of 0.265, 0.255, and 0.245 were used to calculate R_w at 90, 95, and 100 °C, respectively. The analysis shows that R_w in the H_{II} phase decreases with temperature, as was observed for the water channel pore size in the cubic phase (compare Figures 7 and 8). Specifically, the water channel is 15.1 Å in diameter at 90 °C and 14 Å at 100 °C (Figure 8). This represents an average decrease of about 0.1 Å/°C. The corresponding value in the *Pn*3*m* phase in the 50−80 °C range is 0.1−0.2 Å/°C. Since water channel radius in both the H_{II} and *Pn*3*m* phases is dependent on Φ_w, the hydration limit of the phase, it is not unreasonable to find that aqueous pore size decreases with temperature. This thermal response no doubt reflects a shifting of the excess water boundary to lower hydration levels as temperature increases (Figure 2). In contrast to the *Pn*3*m* phase, lipid length in the fully hydrated H_{II} phase is relatively temperature insensitive, with an *l*-value of ca. 13 Å in the 90−100 °C range. In the *Pn*3*m*, *l* drops at an average rate of ca. 0.05 Å/°C from an initial value of ca. 16 Å at 50 °C to ca. 15 Å at 80 °C.

4.5. Correlation Between Molecular Structure and Phase Behavior. A primary objective of this research program is to explore the relationship between molecular structure and mesophase behavior by comparing *T*−*C* phase diagrams for a series of homologous lipid molecules. In this paper, the emphasis is on understanding the effect that double-bond position along the acyl chain has on the phase behavior of monounsaturated monoacylglycerols. Accordingly, a comparison has been made between monovaccenin and monoolein with a double bond at C11 and C9, respectively. The *T*−*C* phase diagram of the monoolein/water system is already available.[3,17−19] However, controversy prevails for this system at temperatures below 30 °C. Accordingly, we will restrict the comparison between the phase diagrams of monovaccenin (Figure 2) and monoolein (Figure 4B)[3] to temperatures above 30 °C.

Monovaccenin and monoolein both exhibit the same phases in the same order with respect to temperature and hydration, with similar structure parameters and temperature and composition dependencies. At low hydration values and at low temperatures, at least one L_c phase is found in both systems. The FI phase is formed directly from the dry material upon heating. Increasing sample hydration and temperature results in the formation of the L_α phase. The cubic and H_{II} phases are formed at generally higher hydration and temperature values, respectively, with the H_{II} phase replacing the cubic phases as temperature increases. Additionally, the slopes of the boundaries separating the various phases have the same sign in both systems, although the magnitude of the slopes differ slightly. The upper temperature limit of the liquid crystalline phases is close to 100 °C for both lipids.

While similarities exist, there are obvious differences between the monovaccenin and monoolein phase diagrams, as might be expected since they are distinctly different molecules. The changes seen include phase transition temperatures and phase boundary positions. An elevation of 5 °C in the melting point of the dry monovaccenin (38 °C) is observed compared to monoolein (33 °C). In the monoolein system, the H_{II} phase coexists with bulk water in the temperature range from ca. 90 to 102 °C, while the corresponding stability range for the monovaccenin system is 87 to 105 °C, representing an increase of 6 °C. A significant difference between the monovaccenin and monoolein systems also lies in the position of the various hydration boundaries. Specifically, full hydration occurs at a higher water content in the monovaccenin system at any temperature in the range studied. The increase in water carrying capacity of monovaccenin, which is also reflected in the size of the water channel in the fully hydrated cubic phase (Figure 7), has been rationalized earlier on the basis of dynamically averaged molecular shape. Thus, for example, at 80 °C, the *Pn*3*m* phase is fully hydrated at 29% (w/w) water in monovaccenin. The corresponding value in monoolein is 26% (w/w) water. At 100 °C, the H_{II} phase is fully hydrated at 24% (w/

w) water in the monovaccenin system, while for monoolein, full hydration sets in at 22% (w/w) water. This difference is reflected in the $T-C$ space occupied by different phases. Most obviously, when the double bond moves from C9 to C11, the area of $T-C$ space occupied by the H_{II} phase has almost doubled.

As pointed out in an earlier study on the phase behavior of five homologous monoacylglycerols from this laboratory,[20] longer fatty acyl chains (where length refers to effective lipid length) tend to stabilize nonlamellar structures and lower the water-carrying capacity of the fully hydrated phases. However, the comparison of monovaccenin and monoolein, molecules with similar effective lipid lengths in the liquid crystalline phase but quite different water-carrying capacities, emphasizes the need to consider molecular shape, which can be characterized by γ, the shape factor, when describing mesomorphism. As noted above, monovaccenin has the smaller shape factor of the two molecules for a given value of l and, in effect, is "slimmer" in shape. The net result is that it tends to form less highly curved structures that hold more water. The slimmer shape attributed to monovaccenin as compared to monoolein reveals itself as having a larger water channel radius in the fully hydrated cubic phase, and also as a shifting of the $Pn3m/(Pn3m + H_2O)$ and $H_{II}/(H_{II} + H_2O)$ boundaries to higher water concentrations in the $T-C$ phase diagram. An important conclusion from this work is that in order to understand the relationship between molecular structure and phase behavior, both the lipid length and the lipid shape must be considered.

4.6. Controlled Drug Release. A knowledge of the phase behavior of the monoacylglycerol/water systems can be used to guide the design of controlled drug release systems based on the lamellar, hexagonal, or cubic phases they form.[21,22] The unique bicontinuous structure of the cubic phases makes them especially attractive for use as a controlled release matrix. Studies have shown that small molecule drugs, incorporated into the cubic phases formed by monoacylglycerols in excess water, are released slowly over a period of hours to days, thereby improving the performance of the drug.[23−25] For certain drugs, a sustained release is preferable to immediate release coupled with repeated administration. Since release rates are modulated by the size of the pores that permeate such materials,[26] the ability to adjust pore size at will affords the opportunity of customizing release rate. This study shows clearly that cubic phase pore size can be changed by selecting different monoacylglycerol lipids and/or by adjusting conditions such as temperature and composition (Figure 7). Monovaccenin and monoolein together provide an excellent system for studying the effect of water channel size on release properties, because of their close resemblance in molecular structure and indistinguishable effective molecular length, yet they display distinctly different water channel pore sizes. Work along these lines is already in progress with the aim of understanding and exploiting the mechanism of drug release in cubic phases. Other means of controlling the release profile from cubic phases make use of lipid mixtures and mesophases incorporating biodegradable polymers.

4.7. Crystallization. Cubic phases have been used recently to procure crystals of a variety of materials ranging from simple salts through to water-soluble and integral membrane proteins.[7−10] The exact role played by the cubic phase medium in such applications, particularly membrane protein crystal formation, is not understood. However, the prospect exists that cubic phases provide the conduit to membrane protein crystals and, thus, three-dimensional protein structures. Accordingly, the onus exists to decipher the role played by the cubic phase in such processes to more efficiently use them and extend their range of applicability. To do so, it is imperative that we establish how mesophase behavior and structure are influenced first by lipid composition and subsequently by the presence of proteins and other additives. The current work represents a step in this direction. The monovaccenin system has now been characterized in terms of its equilibrium phase behavior and phase microstructure. It, along with the other monoacylglycerols that have been examined in comparable detail, provides a series of lipids wherein the cubic phase structure can be manipulated in a systematic way with a view to uncovering the crystallization mechanism and extending its range of usefulness.

5. Conclusions

In this paper, we report the temperature−composition phase diagram of the monovaccenin/water system as constructed using X-ray diffraction for purposes of phase identification and structure characterization. The phase diagram is similar in many respects to that of a related monoacylglycerol, monoolein. The differences however, highlight the relationship between lipid molecular structure and phase behavior, and in particular how effective lipid length and lipid shape influence mesophase microstructure. Comparing monovaccenin and monoolein, monoacylglycerols with the same acyl chain length, we find that shifting the cis double bond away from the glycerol headgroup produces a "slimmer" molecular shape, the effect of which is to stabilize a less curved polar/apolar interface and to increase the water-carrying capacity of the phase. The issue of nonequilibrium phase behavior was addressed in this study particularly as it relates to the liquid crystalline phases at low temperatures where transport may kinetically limit the attainment of equilibrium. In the case of monovaccenin, undercooling was avoided by incubating samples at −10 °C for 2 h before measurement. The importance of cubic phases as controlled-release drug carriers and crystallization media was discussed. Our results show that monovaccenin should play a role in such applications by providing a larger water channel radius without affecting lipid bilayer thickness in comparison to monoolein.

Acknowledgment. We thank the staff at the X9B line of NSLS for their assistance at the beamline. This work was supported by grants from the Sigma Xi Grants-in-Aid of Research, the National Institutes of Health (DK 36849 and DK 45295), and the National Science Foundation (DIR 9016683). Thanks also go to members of our research group for valuable input on this manuscript.

References and Notes

(1) Briggs, J.; Caffrey, M. *Biophys. J.* **1994**, *66*, 573−587.
(2) Briggs, J.; Caffrey, M. *Biophys. J.* **1994**, *67*, 1594−1602.
(3) Briggs, J.; Chung, H.; Caffrey, M. *J. Phys. II* **1996**, *6*, 723−751.
(4) Qiu, H.; Caffrey, M. *Biophys. J.* **1995**, *68*, A431.
(5) Eriksson, P. O.; Lindblom, G. *Biophys. J* **1993**, *64*, 129−136.
(6) Ljusberg-Wahren, H.; Nyberg, L.; Larsson, K. *Chim. Oggi* **1996**, *14*, 40−43.
(7) Landau, E. M.; Rummel, G.; Cowan-Jacob, S. W.; Rosenbusch, J. P. *J. Phys. Chem. B* **1997**, *101*, 1935−1937.
(8) Yang, J. P.; Qadri, S. B.; Ratna, B. R. *J. Phys. Chem.* **1996**, *100*, 17255−17259.
(9) Pebay-Peyroula, E.; Rummel, G.; Rosenbusch, J. P.; Landau, E. M. *Science* **1997**, *277*, 1676−1681.
(10) Landau, E. M.; Rosenbusch, J. P. *Proc. Natl. Acad. Sci. U.S.A.* **1996**, *93*, 14532−14535.
(11) Razumas, V.; Kanapienienė, J.; Nylander, T.; Engström, S.; Larsson, K. *Anal. Chim. Acta* **1994**, *289*, 155−162.
(12) Anderson, D. M.; Gruner, S. M.; Leibler, S. *Proc. Natl. Acad. Sci. U.S.A.* **1988**, *85*, 5364−5368.

(13) Turner, D. C.; Wang, Z.-G.; Gruner, S. M.; Mannock, D. A.; McElhaney, R. N. *J. Phys. II* **1992**, *2*, 2039−2063.
(14) Gulik, A.; Luzzati, V.; DeRosa, M.; Gambacorta, A. *J. Mol. Biol.* **1985**, *182*, 131.
(15) Israelachvili, J. *Intermolecular & Surface Forces*, 2nd ed.; Academic Press Inc.: San Diego, CA, 1991.
(16) Seddon, J. M. *Biochim. Biophys. Acta* **1990**, *1031*, 1−69.
(17) Hyde, S.; Andersson, S.; Ericsson, B.; Larsson, K. *Z. Kristallogr.* **1984**, *168*, 213-219.
(18) Lutton, E. S. *J. Am. Oil Chem. Soc.* **1965**, *42*, 1068−1070.
(19) Aomori, H.; Ishiguro, T.; Kuwata, K.; Kaneko, T.; Ogino, K. *Yukagaku* **1995**, *44*, 1004−1011.
(20) Briggs, J. The phase behavior of hydrated monoacylglycerols and the design of an X-ray compatible scanning calorimeter. Ph.D. Thesis, The Ohio State University, 1994.
(21) Burrows, R.; Collett, J. H.; Attwood, D. *Int. J. Pharm.* **1994**, *111*, 283−293.
(22) Engström, S.; Lindahl, L.; Wallin, R.; Engblom, J. *Int. J. Pharm.* **1992**, *86*, 137−145.
(23) Wyatt, D.; Dorschel, D. *Pharm. Technol.* **1992**, *16*, 116, 118, 120, 122, 130.
(24) Engström, S. *Polym. Prepr.* **1990**, *31*, 157−158.
(25) Puvvada, S.; Qadri, S. B.; Naciri, J.; Ratna, B. R. *J. Phys. Chem.* **1993**, *97*, 11103−11107.
(26) Deen, W. M. *AIChE J.* **1987**, *33*, 1409−1424.